# Pickering stabilization of thymol through green emulsification using soluble fraction of almond gum – whey protein isolate nano-complexes

*Ali Sedaghat Doost*[*1], Maryam Nikbakht Nasrabadi[1,2], Vincent Kassozi[1], Koen Dewettinck[3], Christian V. Stevens[4], Paul Van der Meeren[1]*

[1]*Particle and Interfacial Technology group, Department of Green Chemistry and Technology, Faculty of Bioscience Engineering, Ghent University, Coupure Links 653, 9000, Gent, Belgium*

[2]*Department of Food Science and Technology, College of Agriculture, Isfahan University of Technology, Isfahan 84156-83111, Iran*

[3]*Laboratory of Food Technology and Engineering, Department of Food Technology, Safety and Health, Faculty of Bioscience Engineering, Ghent University, Coupure Links 653, 9000, Gent, Belgium*

[4]*SynBioC Research Group, Department of Green Chemistry and Technology, Faculty of Bioscience Engineering, Ghent University, Coupure Links 653, 9000, Gent, Belgium*

## Abstract

In this study, the soluble fraction of almond gum (SFAG) as a sustainable biopolymer source and whey protein isolate (WPI) were used for self-assembly preparation of SFAG-WPI nano-complexes through electrostatic interaction. The SFAG was characterized using $^{1}H$ and $^{13}C$ NMR. The influence of total biopolymer concentration (0.2-0.4 %w/v) and ratios (1:3-3:1) as well as of the pH (2-6) on the formation of complexes was established by visual, light scattering, surface charge, and spectrometric observations. The outcomes proved the formation of negatively charged soluble complexes in the range of pH 4-5 and insoluble complexes at pH values 3 to 4. The soluble coacervate particles at pH 4.5 and total concentration of 0.4 %w/v were selected to induce Pickering stabilization of thymol. The static light scattering with microscopy studies (CLSM and Cryo-SEM) showed the formation of thymol oil-in-water emulsions by adsorption of nano-complexes on the surface of the droplets. Thymol emulsions stabilized using complexes had no size variation under storage (40 days) with an opaque and homogenous appearance. On the other hand, the emulsions containing solely WPI at pH 4.5 showed a substantial droplet size increase with severe creaming. Droplet size analysis together with coalescence and flocculation indices presented that coalescence was mainly responsible for droplet size coarsening of the emulsions stabilized by native WPI at pH 4.5. Overall, our outcomes indicated the improvement of WPI in the stabilization of emulsions through complexation.

*Keywords:*

*Self-assembly, coacervate, Pickering stabilization, almond gum, whey protein isolate, thymol.*

**Corresponding author:* Ali Sedaghat Doost

*Email:* ali.sedaghatdoost@ugent.be, ali.sedaghatdoost@gmail.com

*Address:* Particle and Interfacial Technology group, Department of Green Chemistry and Technology, Faculty of Bioscience Engineering, Ghent University, Coupure Links 653, 9000, Gent, Belgium

Tel: +32 (0)9 264 60 04

## 1. Introduction

There is an increasing consumer demand for more natural and environmentally friendly products known as ‘‘clean label’’ products including foods, cosmetics and pharmaceuticals. Proteins and polysaccharides are natural polymers that are widely used as functional ingredients in different products, primarily foods. These biopolymers are capable of stabilizing emulsions and foams, thickening solutions, and forming gels (McClements & Gumus, 2016). As the properties of individual biopolymers can be altered by different conditions, for instance, pH or ionic strength, there is a particular interest in the use of polysaccharide–protein complexes in order to improve their functional properties. Maillard conjugates and electrostatic complexes are major complexation of proteins and polysaccharides (McClements & Gumus, 2016; Semenova, 2017). Recently, these types of particles have been the subject of several studies due to their green and straightforward preparation, as well as biopolymer based materials and economic costs.

Low and high molecular weight surfactants have been extensively used to stabilize emulsions but there has been recently a great demand for the Pickering emulsions. These emulsions are conventionally stabilized using solid particles, which have partial wettability to two lipid and aqueous phases (Ettelaie, Zengin, & Lishchuk, 2017; Wang & Heuzey, 2016). Colloidal complexes with partial wettability, which are able to accumulate at the interface to prevent coalescence or Ostwald ripening can be utilized to induce the Pickering stabilization (Ettelaie & Murray, 2015; Lu, Zhang, Li, & Huang, 2018). To this end, the soluble fraction of almond gum (SFAG) - whey protein isolate (WPI) colloidal complexes were established.

Almond gum is a high molecular weight biopolymer, which exudates from almond gum trees (*Amygdalus communis L.*) (Sedaghat Doost, Muhammad, Stevens, Dewettinck, & Van der Meeren, 2018). This gum consists of a water soluble and a water insoluble fraction. The water soluble fraction constitutes about 90% of the almond gum with the highest total sugar content (93%) and the insoluble fraction contains more protein and fat than the soluble fraction (Rezaei, Nasirpour, & Tavanai, 2016). SFAG contains uronic acid and sugar analysis indicated that arabinose and galactose are the main monosaccharides present in almond gum. The great advantage of SFAG over common gums is its simple production. This gum exudates from almond trees as a consequence of mechanical injury. Therefore, the sustained production source attracts attention (Mahfoudhi, Chouaibi, Donsì, Ferrari, & Hamdi, 2012). SFAG has a high potential for application as a preservative or stabilizer in the food industry because of its low cost, high availability, and high water absorption capacity (Mahfoudhi et al., 2012; Rezaei et al., 2016).

Whey protein isolate is a value-added ingredient sensitive to pH conditions and low thermal stability due to the denaturation, which can be improved through electrostatic complexation (Wagoner &

Foegeding, 2017). Whey protein is originally a cheese processing byproduct containing a mixture of proteins mainly $\beta$-lactoglobulin (Wu et al., 2015). A wide range of isoelectric points (IEP) has been reported for WPI (4.2 – 5.2) (Akhtar & Dickinson, 2007; Pelegrine & Gasparetto, 2005; Setiowati, Saeedi, Wijaya, & Van der Meeren, 2017). Typically, the proteins are positively charged below the IEP while they are negatively charged above their IEP. This characteristic can be exploited for the formation of particles through electrostatic interaction when a combination of a protein below its IEP and an anionic polysaccharide are mixed together, leading to the self-assembly of the polymers (de Kruif, Weinbreck, & de Vries, 2004; Ye, 2008).

Thymol (2-isopropyl-5-methylphenol) as a major constituent of some essential oils, is a phytophenolic (monoterpene) compound found mainly in *Thymus vulgaris L*. and *Origanum vulgare L.* (Deng, Taxipalati, Que, & Zhang, 2016; Sedaghat Doost, Devlieghere, Dirckx, & Van der Meeren, 2018). Thymol is used widely in different products owing to its antibacterial, antifungal, antioxidant, and anticancer properties (de Castro et al., 2015; Kang et al., 2016; Liolios, Gortzi, Lalas, Tsaknis, & Chinou, 2009; Sedaghat Doost, Dewettinck, Devlieghere, & Van der Meeren, 2018; Yanishlieva, Marinova, Gordon, & Raneva, 1999). The hydrophobicity, crystal powder form, and strong flavor of this compound have limited its exploitation. Therefore, it has to be encapsulated within a delivery system. Previous studies prepared carrying systems for thymol by dissolving it in an organic solvent such as ethanol or propylene glycol. However, these formulations have their own detrimental effects such as their synthetic nature (J. Li, Chang, Saenger, & Deering, 2017; Su & Zhong, 2016). As the aim of this study was to design a solely natural system, an attempt was made to formulate colloidal dispersions using food grade and green solvents. To this end, thymol was mixed with tricaprylin oil (TCA) as a medium chain triglyceride, which is used as penetration promoter and emollient.

The purpose of this study was to produce WPI-SFAG colloidal coacervate particles through electrostatic interaction. Moreover, the appropriate conditions for nanoparticle preparation were obtained by the formation of SFAG-WPI complexes at different pH conditions, ratios and total biopolymer concentrations. Then, an attempt was made to prepare Pickering stabilized thymol emulsions using the prepared bioparticles.

The novelty of this study lies in the use of SFAG as a novel hydrocolloid and the green emulsification technique of thymol using self-assembled nanoparticles. Our work provides practical and theoretical information about the Pickering stabilization of thymol. These findings provide a way to design ''surfactant free'' products from sustainable natural sources for variable applications such as in food, health care, and cosmetics.

## 2. Materials and methods

### 2.1. Materials

Almond gum was provided by Sepahan Nano-Food Co. (Isfahan, Iran). The provided sample had a white colour and a uniform size and was collected from similar types of trees (*Amygdalus communis L.*). WPI was provided by Davisco Foods International Inc. Bipro (Le Suer, MN, USA). The protein content of this product has been previously reported to be 92.6% consisting of 85% $\beta$-lactoglobulin (Van der Meeren, El-Bakry, Neirynck, & Noppe, 2005). Thymol (2-isopropyl-5-methylphenol) was purchased from Sigma-Aldrich Co (St. Louis, MO, USA). Tricaprylin (TCA) oil is commercially available as Miglyol®808 (caprylic acid with a purity of > 95%) and was provided by IOI Oleo GmbH (Witten, Germany).

### 2.2. Extraction and characterization of the soluble fraction of almond gum

#### 2.2.1. Extraction

The soluble fraction of almond gum (SFAG) was extracted using the method previously described by (Sedaghat Doost et al., 2018). Briefly, a stock solution of SFAG (4 % w/v) was prepared in distilled water left to be mixed for 3h at ambient temperature (20°C). The mixture was stored at 4°C overnight before centrifugation at 44814g for 30min at 25°C. Sodium azide was added to the solution (0.02 % w/v) in order to prevent microbial growth. The concentration of the extract was determined by means of drying a certain amount at 105°C overnight. This experiment was performed after each extraction.

#### 2.2.2. 1-D nuclear magnetic resonance ($^{1}$H, $^{13}$C NMR)

The $^{1}$H and $^{13}$C NMR spectra of SFAG was obtained using a Bruker Avance III Nanobay 400 MHz spectrometer equipped with a 5mm PABBO BB probe at 30°C. The SFAG solution was dried inside a freeze-drier (Alpha 1-2 LD plus, Christ) and it was dissolved in $D_2O$ (0.5%w/v) containing 5mM sodium acetate as an internal standard and the proton spectrum was recorded. The $^{13}$C spectrum of 2 % w/v SFAG (20mM sodium acetate) was acquired at 100.6MHz for 72h.

#### 2.2.3. Proximate analysis

The moisture, fat, and ash content of SFAG was determined according to the standard AOAC methods (2003). Protein content was determined based on the DUMAS combustion method using an Elemental Analyzer - Isotope Ratio Mass Spectrometer (EA-IRMS) (20–22, SerCon, Cheshire, UK). Samples were placed into tin foil capsules for combustion under a purge of He gas at 1000°C. A calibration curve was made with a known standard concentration (0-15 µl) of ammonium sulphate. The nitrogen (N) content was calculated by the comparison of the area under the curve obtained from the standard and the sample. A casein solution with a known concentration was utilized as a control. The nitrogen content was converted to the protein content by multiplication by 6.25.

The carbohydrate content was obtained by the difference between the sum of the other components and 100%. All the measurements were carried out in triplicate and the average ± standard deviation

(STD) were reported.

### 2.3. SFAG-WPI complex formation and characterization

#### 2.3.1. Complex preparation

A WPI stock solution was prepared by dissolving 2g in 100ml of 10mM acetate buffer at pH 6 (2 % w/v). The mixture was left on a stirrer for 3h at room temperature (20°C) and stored in a refrigerator (4°C) for further analyses. WPI and SFAG solutions were mixed together at different ratios (0:3, 1:3, 2:3, 3:3, 3:2, 3:1, 3:0) at a total concentration (TC) of 0.4 or 0.2 % w/v. The pH of the solutions was adjusted to 2-6 by adding dropwise of NaOH or HCl (0.1M).

#### 2.3.2. Particle size and surface charge determination

The size distribution of the complexes was measured using Photon Correlation Spectroscopy (Model 4700, Malvern Instruments, U.K.) at a scattering angle of 150° at 25°C. The sample was diluted prior to analysis with an appropriate solution (of the same pH) to avoid multiple scattering. The light intensity correlation function was analyzed based on the multimodal method whereas the z-average diameter was obtained by cumulant analysis. Each individual measurement was an average of 10 runs. The reported value is the mean of three measurements ± STD.

The zeta potential (ζ) of the complex particles was determined using a Zetasizer 2c (Malvern Ltd, UK) by measuring the electrophoretic mobility using the Smoluchowski approximation. The samples were diluted prior to analysis. The reported values are the mean of three repetitions ± STD.

#### 2.3.3. Optical turbidity

Turbidity measurements were employed to identify the possible structural transitions associated with the formation of soluble and insoluble complexes using a UV-visible spectrophotometer (VWR, Belgium) at 600nm. 10mM sodium acetate buffer was used as a blank reference. All these measurements were carried out in triplicate using separate stock solutions.

#### 2.3.4. Charge titration

The SFAG solution (0.16%w/v), WPI (0.24%w/v), and the mixed solution of WPI:SFAG (3:2, TC= 0.4 % w/v) was titrated using HCl/NaOH (0.1M) from pH 6 to 2 and the streaming potential was read utilizing a Charge Analyser II (Rank Brothers Ltd, England).

#### 2.3.5. Contact angle

Solutions of WPI as well as SFAG and WPI:SFAG nanoparticles (3:2, TC = 0.4 % w/v) were prepared at pH 4.5 (10mM sodium acetate buffer). The samples were lyophilized using a freeze-drier (Alpha 1-2 LD plus, Christ). The powders were pressed at 89.2MPa to form a tablet of 15×50mm using a hydraulic press. The contact angle was measured utilizing a drop shape analyzer (DSA, Krüss, Germany) by

dripping a sodium acetate buffer (10mM) droplet (10µl) at pH 4.5 on the tablet; the contact angle was automatically calculated using Young-Laplace equation by the software.

### 2.4. Pickering stabilized emulsion preparation

The oil-in-water emulsions were prepared by weighing 4g of thymol and TCA oil mixture and 96g aqueous phase containing either SFAG (0.16%w/v), WPI (0.24%w/v), or SFAG:WPI complex (0.16:0.24%w/v) dissolved in 10mM acetate buffer (pH 4.5). The lipid phase mixture consisted of thymol and TCA at a ratio of 4:1 (this ratio was selected based on trials) heated to 60°C for complete melting of thymol crystals and left for 1h on the stirrer at room temperature (20°C). The liquid oil mixture and aqueous mixtures were then homogenized using a high speed blender Ultra-Turrax T25 (Germany) at 24000rpm for 5min. The emulsions were kept at 4°C for further analyses. The pH of emulsions after preparation was adjusted if it was needed.

### 2.5. Emulsion characterization

#### 2.5.1. Droplet size determination

The droplet size distribution of the samples was measured using static light scattering. A Mastersizer 3000 (Model 3000 Hydro MV, Malvern Instruments, UK) was used to determine the volume-weighted mean diameter (d[4,3]) of the samples at 20°C. The samples were characterized by a refractive index of 1.45 and 1.33 for the oil phase and acetate buffer (10mM), respectively, with an absorption of 0.01. A few droplets of the sample was added into the wet dispersion unit containing acetate buffer (10mM) at pH 4.5. The measurement was run at a dispersion speed of 1500rpm for 10s. Each individual measurement was an average of three runs.

#### 2.5.2. Flocculation and coalescence indices

The flocculation and coalescence indices of the emulsions were calculated as follows:

$$\text{Flocculation index (FI)} = \left[\left(\frac{d40\ [4,3]}{d40\ [4,3](SDS)}\right) - 1\right] \times 100$$

$$\text{Coalescence index (CI)} = \left[\left(1 - \frac{SSA40\ (SDS)}{SSA0\ (SDS)}\right)\right] \times 100$$

where d[4,3] was measured on day 40 ($d_{40}$) storage diluted in acetate buffer (10mM, pH 4.5) with and without 1% SDS and the specific surface area (SSA in $m^2$/ml) was calculated from the Sauter mean diameter d[3,2] at day 0 and 40 diluted in acetate buffer (10mM, pH 4.5) with SDS (1%) (Castellani, Belhomme, David-Briand, Guérin-Dubiard, & Anton, 2006).

#### 2.5.3. Microscopy studies of microstructure

The morphology and formation of thymol emulsions was evaluated using a Cryo-SEM (JSM-7100, Jeol Europe, Belgium) equipped with a PP3000T device (Quorum Technologies, East Sussex, UK). A small

amount of sample was placed on a copper grid. The sample was frozen in a nitrogen slush (-190°C) followed by fracturing. Then, it was sublimated and sputter coated with platinum prior to photograph recording.

Confocal laser scanning microscopy (CLSM) (Leica TCS-SP5, Germany) was utilized to visualize thymol Pickering stabilized emulsions. WPI-SFAG nanoparticles (3:2, pH 4.5, TC = 0.4) and oil phase were stained by Rhodamine B and Nile red, respectively. The excitation and emission wavelengths of Rhodamine B were set as 560 and 625nm, respectively. Nile red was excited at 488nm and detected at 680-700nm. The emulsions after staining were diluted by the appropriate acetate buffer in order to have individual emulsion droplet. The images were processed using Image J software.

#### 2.5.4. Interfacial tension measurements

The interfacial activity at the interface of oil (thymol:TCA = 4:1) and WPI (0.24%w/v) and SFAG:WPI complex (0.16:0.24%w/v) solutions was determined using an automated drop shape tensiometer (Tracker, Teclis, I.T.C., France). The calibration of the tensiometer was performed by measuring the surface tension of Milli-Q water (72 ± 0.4 mN/m, 25°C). A pendent needle was used to create a droplet of a solution of either WPI or complexes into a cuvette filled with the oil. The density of the samples was measured using an Anton-Paar DM5000 density meter at different temperatures.
As the density has a major impact on these measurements, a water bath was connected to the cuvette holder to keep the temperature constant at 25°C.

### 2.6. Statistical analysis

The reported values are the mean ± standard deviation of at least two repetitions. One-way analysis of variance (ANOVA) was used for all statistical analyses to determine significant differences of means ($P < 0.05$).

## 3. Results and discussion

### 3.1. Purification and chemical composition of SFAG

The water soluble fraction of almond gum (SFAG) was purified by centrifugation and it was used for the formation of complex coacervates with whey protein isolate (WPI). Initially, the chemical composition of SFAG was determined by proximate analyses. The ash, fat and moisture content were found to be 1.0 ± 0.2, 0.5 ± 0.1, and 3.3 ± 0.7 %, respectively; these values are in good agreement with previously reported results (Mahfoudhi et al., 2012; Rezaei et al., 2016; Sedaghat Doost et al., 2018) . In accordance with the previous results of Mahfoudhi et al. (2012), a trace amount of protein (2.3 %) was detected by the DUMAS method in the SFAG. The results revealed that the major constituent (92.9 %) of the SFAG was carbohydrates.

In order to have a better understanding of the chemical composition of the SFAG, the NMR spectra

($^{1}$H, $^{13}$C), shown in Figure 1 a&b, were also recorded. The peaks in the proton spectrum at 4.7 and 1.9 ppm were assigned to deuterated water and sodium acetate, respectively. The small triplet proton signals around 1.2 ppm in the spectrum could be related to the methyl group of rhamnose. The crowded signal region between the chemical shifts of 3.3 and 5.3 ppm is typical for polysaccharides, indicating the presence of similar sugars. It has been shown that SFAG is an arabinogalactan polysaccharide consisting of around 47 % arabinose and 35 % galactose (Rezaei et al., 2016). This region consisted of two non-anomeric (3.3-4.6 ppm) and anomeric (4.8-5.8 ppm) signals, which can not be distinguished well due to the overlapping of the peaks. The signal at around 5.2 ppm could be attributed to the anomeric protons linked to Araf and the peak at 5.05 ppm for the $\boldsymbol{\alpha}$-Araf non-reducing terminal (Nosalova et al., 2013). Galactopyranose signal peaks were also observed at the chemical shifts around 4.2, 3.7 and 3.4 ppm, respectively (Izumi, 1977).

The $^{13}$C NMR spectrum has the advantage that the peaks are distributed over a broader range than the $^{1}$H NMR spectrum, meaning that it suffers less from overlapping. Typically, the signals at 60 to 85 ppm can be assigned to non-anomeric carbons while anomeric carbons have peaks at around 90 to 110 ppm (Cui, 2005). The peaks observed in the range of 101 - 103 ppm can be related to the (1-->6)-linked galactopyranosyl residues, which is in good agreement with the $^{1}$H NMR spectrum (Karácsonyi, Kováčik, Alföldi, & Kubačková, 1984). The $^{13}$C NMR spectrum displayed peaks of *Araf* from 107.6 to 109.7 ppm and C-2 of Araf at 83.7 ppm (Willför, Sjöholm, Laine, & Holmbom, 2002). The spectrum also exhibited a pronounced peak at 103.2 ppm related to *Galp* and a peak around 75.04 ppm attributed to xylose (Simas-Tosin et al., 2009). In accordance to the previous studies showing that SFAG contains uronic acid, the peak around 176 ppm offered the carboxylic group (-COOH) signal peak of uronic acid (Mahfoudhi et al., 2012; Sedaghat Doost et al., 2018).

Overall, these results were in good agreement with the results obtained by Rezaei et al. (2016) who studied the fractionation and chemical composition of a similar type of almond gum.

### 3.2. Biopolymer particle formation

#### 3.2.1. Optical turbidity

Initially, the formation of particles due to the interaction between SFAG and WPI at different pH conditions as well as protein to polysaccharide ratio and total biopolymer concentration was examined.

The optical turbidity profile of the acid titration of a protein and polysaccharide combination could be utilized to establish the possible complex formation due to the structural transition. The visual appearance assessment of a WPI and SFAG mixture at a ratio of 3:2 and TC = 0.2 and 0.4 % w/v at varying pH (2-6) showed that precipitation occurred between pH 2.5 and 4 (the precipitation of the mixture at pH 4 occurred at longer times) (Figure 2a, red arrows). This indicated the associative phase

separation due to the electrical neutralization of strong opposite charges of the WPI and SFAG, which led to the self-assembly of large particles and thereby the formation of insoluble complex coacervates (Dickinson, 1998). On the other hand, a very clear solution was visible at pH $\leq$ 2, which can be attributed to the highly protonated functional groups of SFAG and WPI leading to strong electrostatic repulsion between two polymers. Similarly, at pH > 5, the polymer mixtures had a transparent appearance presenting segregative phase separation of two similarly charged polymers. $\boldsymbol{\beta}$-lactoglobulin as a major constituent of WPI contains Leu, Val, and Ile amino acid residues within its chemical structure. The $\boldsymbol{\alpha}$-carboxylic (-COOH) and –amino (-$NH_2$) acid moieties of these amino acids and carboxylic groups of SFAG would be protonated or deprotonated at extremely low and high pH values, respectively, giving rise to the segregative phase separation (Dickinson, 2005).

Opaque and homogenous mixtures were on the other hand observed at pH > 4.2 transferring to fully transparent mixtures at pH > 5. In fact, Pelegrine and Gasparetto (2005) found the IEP of WPI to be 4.5. Although based on this IEP (4.5) WPI has overall no net charges, there still exist some amino groups with positive charges which can readily interact with carboxylic groups of SFAG at the IEP. Therefore, an electrostatic interaction at the IEP could be expected as it was observed by the visual turbidity. Nevertheless, as the pH increased both the reactive groups of WPI and SFAG became greatly negative and similarly to pH 2 the electrostatic repulsion between like charges inhibited interaction. A similar trend was obtained at a total concentration of 0.2 % w/v at different pH conditions but with less visual turbidity at pH 4-5, which was due to the fact that at the lower concentration of the biopolymers either the number and/or the size of the created particles was smaller leading to less turbidity of the mixtures (Figure 2a).

The results obtained from the turbidity analyses of the samples at 600nm (Figure 2b) were consistent with the visual appearance evaluation. The acid titration of the biopolymer mixture from pH 6 to lower pH conditions exhibited a dramatic increase in the optical turbidity from $pH_C$ = 5 reaching to the maximum value at $pH_{opt}$ = 4. $pH_C$ is the pH where soluble intrapolymeric complexes are initiated to form (Turgeon, Beaulieu, Schmitt, & Sanchez, 2003), which was observed by the slight increase in the turbidity values at pH 5. The $pH_{opt}$, for both studied total concentrations, could be attributed to the formation of large insoluble particles and a starting point where insoluble complexes will be dissociated (Figure2b) (Turgeon et al., 2003). The pH$\boldsymbol{\varphi}_1$, where phase separation due to neutralization would occur, was assigned to pH 4.4 because the biopolymer mixtures at this pH started to precipitate under longer storage (Eghbal & Choudhary, 2018). At further titration to lower pH values, the turbidity decreased greatly and a severe phase separation was visually observed. Despite of the fact that the turbidity of the samples at pH < 4 was measured after shaking the samples, the large aggregates sedimented very quickly which led to a fluctuating absorbance reading.

Thus, it seemed challenging to obtain a precise reading of the absorbance because it depends on the strength of shaking and the time of reading in different samples. At pH lower than 2.5, the complexes started to dissociate due to the presence of polymers with similar charges (pH$\varphi_2$). The turbidity profile of the biopolymer mixtures with TC = 0.2 % w/v suggested a fairly similar trend to TC = 0.4 % w/v (Figure 2b); the optical density values were lower (Figure 2b), nonetheless, due to the smaller particle size and/or lower number of formed complexes (Eghbal & Choudhary, 2018). In agreement with the results obtained by Liu, Shim, Wang, and Reaney (2015), the pH where primary soluble complexes started forming was independent of the total biopolymer concentration.

Another factor that can significantly influence the formation and the size of the bioparticles is the ratio of biopolymers (Eghbal & Choudhary, 2018). The turbidity of the polyelectrolyte biopolymer mixtures containing different WPI:SFAG ratios varying from 3:0 to 0:3 was measured (Figure 3). At a first glance, the turbidity of WPI-SFAG mixtures was higher than of either individual WPI or SFAG which is an indication that complexes were formed. Unlike the SFAG solution (0:3, 0.24% w/v) that had a very low optical density at varying pH conditions, the WPI (3:0, 0.24% w/v) turbidity increased from pH 4 to 4.5 followed by leveling off up to pH 5. Considering the fact that at the IEP, the aggregation of proteins occurs, relatively high turbidity values were obtained in the range of 4.5 to 5. The samples providing more SFAG to the WPI molecules had a lower turbidity, indicating that there were either no sufficient WPI molecules to interact with SFAG and a smaller number of the particles was formed or particles with a smaller size were created. By contrast, the polymer mixtures with more WPI content had higher turbidity values. This was not surprising because there was no sufficient amount of SFAG molecules to prevent the aggregation of WPI molecules bringing the formation of larger molecules about and thereby higher turbidity.

### 3.2.2. Particle size and surface charge properties

The particle size distribution of the formed coacervates at a WPI to SFAG ratio of 3:2 (TC = 0.4 % w/v) was evaluated as a function of pH (Figure 4a). Two particle size regimes were observed. Coacervate particles were found to have a large z-average diameter at pH 4 explaining the higher turbidity values obtained at this pH. Below the IEP, the $-NH_2$ groups present within the chemical structure of WPI are protonated. Hence, an interaction is achieved with the negatively charged moieties of AG. A size reduction regime was visible up to pH 4.5 where the second regime was started. By further pH increase to 5, the size of the particles significantly ($P < 0.05$) decreased to a smaller mean particle diameter, indicating that more negative charges at pH > IEP provide repulsion between the polymers which led to the dissociation of the formed complexes and thereby the formation of smaller particles. PDI results (Figure 4b) were also in line with the size measurement outcomes. At higher pH values than 4.5, the PDI had a substantial growth, which is an indication that the number of the formed

complexes was very small and they started to break down or form irregular shapes. This effect led to the presence of insufficient light scattering and thereby high PDI values. This observation was in agreement with the optical density results, where the complexes had a less opaque appearance. The particle size measurement of native WPI using DLS in this pH range (4-5) was troublesome due to the very low scattered intensity, which was dominated by (a minor fraction of) large aggregates. The aggregation of protein around and at the IEP is a complex phenomenon, which is attributed to hydrophobic, Van der Waals, and electrostatic attractions. This can explain the aggregation and precipitation of WPI in a pH range of 4-5. Overall, it can be concluded that the interaction of SFAG with WPI molecules inhibited the aggregation of WPI by the formation of complex coacervates. This was confirmed by turbidity and light scattering experiments.

The electrical surface charge properties of proteins measured at different pH values could be used to determine the IEP as there is no net charge at this point. As it can be seen from Figure 4c, the zeta potential of the WPI was +19mV at pH 4, decreasing to almost 0 at a pH around 5 and started to become negative at pH values higher than 5. For comparison, Pelegrine and Gasparetto (2005) figured out that the IEP of WPI was 4.5, while Setiowati et al. (2017) reported 5 is the IEP. In fact, the IEP depends strongly on the WPI composition and on the technique by which the IEP is determined. Surface charge values calculated using electrophoretic mobility measurements revealed that the zero net charge of WPI was obtained at pH 5. On the other hand, at around pH 5.2 the streaming potential approached zero (Figure 4d).

A different behavior was observed when WPI and SFAG were mixed at a ratio of 3:2. At a pH range of 4 to 5.5, they were negatively charged with values varying between -30 to -40mV showing the negatively charged nature of the particles. Thus, it is evident that the addition of gum stabilized WPI against aggregation by increasing the surface charge. This was also confirmed by measuring the streaming potential (Figure 4d) of native WPI as well as of SFAG and WPI:SFAG (3:2, TC = 0.4 % w/v) at different pH conditions. SFAG was negatively charged during the whole range of studied pH values down to 2.2, where zeta potential became zero due to the protonation of the functional groups. The negative values of the streaming potential of SFAG over the studied pH range indicated the anionic nature of almond gum that could be attributed to the uronic acid content of this gum. These results together were consistent with optical density outcomes which revealed that insoluble complexes were formed at pH $\geq$ 2.5. It has been indeed previously reported that the –COOH group has $pK_a < 2$ (Liu et al., 2015). Interestingly, the complexes of WPI and SFAG had no net surface charges around pH 3.8, consistent with turbidity measurements. It was worked out that the precipitation at pH < 4 was due to the formation of insoluble complexes, which was in accordance with the streaming potential outcomes where the surface charge is zero. By further pH reduction, WPI was greatly

protonated while SFAG had negative surface charges leading to rapid neutralization of reactive groups and thereby precipitation.

Overall, it can be concluded that the interaction between WPI and SFAG gave rise to the formation of complex coacervates. We selected a colloidal complex system with WPI to SFAG ratio of 3:2 and TC = 0.4 % w/v at pH 4.5 to prepare thymol emulsions and compare the results with native protein to show the possible improved properties of WPI. This ratio was chosen because consistent with the higher turbidity values compared to the studied ratios, it had a smaller particle size, indicating the formation of a higher number of particles. Ultimately, this pH has been reported as the IEP of WPI where aggregation and precipitation was observed mainly due to the zero net charges, which can be a problem in the stabilization of emulsions.

### 3.3. Pickering emulsion formulation

The wettability and size of the solid particles are the crucial parameters for the formation and stabilization of Pickering emulsions (Xiao, Li, & Huang, 2016). For instance, solid particles should be wetted partially by both phases and their size should be at least 10 times smaller than the targeted size of the emulsions. In the previous section, we showed that the formed nanoparticles (3:2, pH 4.5, TC = 0.4 % w/v) had a z-average particle diameter of 313nm, which can potentially stabilize Pickering emulsions with relatively small diameter.

The contact angle ($\theta$) of native WPI was around 68° at pH 4.5 showing partial wettability, whereas the relatively low contact angle of SFAG (24°) represented its hydrophilic nature. The formation of complexes decreased the water contact angle of native WPI to around 58°, which is not primarily hydrophobic or hydrophilic and thereby appropriate for Pickering stabilization (C. Li, Li, Sun, & Yang, 2013; Wu et al., 2015). In fact, the particles which are going to be positioned at the interface should be able to not only penetrate to the oil phase, but also be hydrated by the aqueous phase. It is believed that particles with a contact angle of 90 would be the ideal case for Pickering stabilization. However, it has been shown in several studies that relatively stable Pickering oil-in-water emulsions can be created by particles with $\theta$ values around 60° (C. Li et al., 2013; Wijaya, Van der Meeren, Wijaya, & Patel, 2017). Thymol oil-in-water emulsions stabilized by only WPI showed a rapid phase separation after a few hours of storage at pH 4.5, but the emulsions containing nano-complexes were opaque and homogeneously dispersed (data not shown). This was not surprising as one would expect that WPI at a pH around the IEP showed aggregation. Therefore, the stabilized emulsions at similar pH conditions would also exhibit aggregation. This aggregation may be re-dispersible at early stages but can potentially lead to the coalescence of the droplets. It is noteworthy to mention that SFAG was not capable to form stable emulsions: the emulsion exhibited very rapid phase separation and oiling-off.

The morphology of the formed emulsions was visualized using Cryo-SEM and confocal microscopy. It was seen from the SEM pictures shown in Figure 5-a that emulsion droplets were successfully formed with a size distribution comparable to the static light scattering measurements. It was also observed through the Cryo-SEM photographs that the globular proteins were captured through the SFAG network responsible for the relatively higher stability of the emulsions.

Confocal laser scanning microscopy (CLSM) of the emulsions stabilized by stained nanoparticles (NPs) using Rhodamin B was employed to visualize the distribution of the particles at the interface. CLSM photos in Figure 5-b&c revealed that the NPs were closely accumulated at the interface of the oil and aqueous phase preventing the coalescence of the oil droplets by creation of a surrounding layer.

The droplet size distribution is an essential microstructure parameter to determine the physicochemical stability of emulsions. Droplet size distribution analyses revealed that the formed emulsions had initially a bimodal distribution when both native WPI and complexes were used. The initial mean droplet diameter (d [4,3]) of the emulsions stabilized by WPI was $5.4 \pm 0.2\mu m$. On the other hand, larger droplets (d [4,3] = $6.5 \pm 0.03\mu m$) were formed when complexes were used for stabilization. It is believed that the complexation could change the conformational properties of WPI and hence, the adsorption properties at the oil-water interface (Wei, Zhu, & Huang, 2018). Moreover, proteins at their IEP have a higher tendency toward the hydrophobic phase due to the lower solubility in the aqueous phase. Thus, the interfacial tension (IFT) changes between oil and an aqueous phase containing either WPI or complexes as a function of time was monitored (Figure 6). In fact, a gradual decrease was observed at first for the adsorption of complexes to the oil phase in order to rearrange their structure in line with the oil phase followed by leveling off. On the other hand, the IFT decreased very rapidly with smooth changes during the comparable measurement time, indicating that WPI adsorbed very rapidly at the oil-water interface. These results suggested that the complexation most probably led to conformational changes of WPI which influenced its adsorption behavior during emulsification. In fact, during mixing, the surfactant should adsorb fast enough to the surface of the newly created droplets to prevent recoalescence of the oil droplets. At a first glance, it seems that native WPI was more efficient in the formation of smaller droplets than the complexes with the reduced adsorption features because of the complexation. However, the droplet size distribution may be potentially varying at longer storage times. In fact, from an industrial and functionality point of view, a product should have sufficient long-term stability. To this end, the droplet size distribution and visual appearance changes were monitored upon storage at 4°C (Figure 7). As it can be seen from Figure 7-a, the thymol emulsions stabilized by only WPI displayed a thick cream layer (a few oil droplets on top), while the Pickering emulsions using NPs were homogenously dispersed.

After 40 days of storage, a substantial shift toward larger sizes in the volume-weighted size

444 distribution of the emulsions containing native WPI was observed. This was consistent with the thick
445 creaming layer optically visible on top of the sample. Nevertheless, there was no sign of
446 physiochemical instability in thymol emulsions stabilized using WPI:SFAG complexes as the droplet
447 size distribution remained unchanged after 40 days of storage (Figure 7-b). In order to examine that
448 the droplet size coarsening in the WPI stabilized emulsions was primarily due to coalescence and not
449 to reversible aggregation, the FI and CI were determined (Castellani et al., 2006). Unlike the thymol
450 emulsions stabilized by native WPI that had a relatively large FI (14.2) at d40, the FI value of the
451 emulsions containing NPs was 0.5. On the other hand, the larger CI (27.8) of the former case
452 suggested that the droplet size growth was due to the combination of flocculation and coalescence
453 of the droplets. Despite the fact that smaller droplets could be formed by the native protein, the WPI
454 molecules (which showed aggregation at pH 4.5) were not able to prevent coalescence and ultimately
455 the emulsion structure broke down. It should be noted that the CI of the emulsions when NPs was
456 used for stabilization, was close to zero (i.e. -0.7). This was in accordance with the electrophoretic
457 mobility of the emulsions containing native WPI which was almost zero explaining the rapid creaming
458 of thymol emulsions due to the aggregation tendency of WPI. This aggregation can promote the
459 rupture of the interfacial layer leading to coalescence. It seemed that the adsorbed proteins with net
460 neutral electrical surface charge were not capable to create sufficient repulsion forces to prevent
461 aggregation leading to creaming and coalescence. On the other hand, the better stabilization of
462 thymol emulsions with complexes adsorbed on the surface could be attributed to electrosteric forces,
463 a combination of electrostatics due to the repulsion between like charges and steric hindrance due
464 to the entropy confining of the chains towards the continuous phase (Sedaghat Doost, Sinnaeve, De
465 Neve, & Van der Meeren, 2017), induced by SFAG molecules. In fact, the interaction of SFAG with
466 WPI could enhance the stability of the formed emulsions via electrosteric stabilization. Overall, it can
467 be concluded that electrostatic complexation of WPI with SFAG can successfully improve the
468 emulsion stabilization of WPI at pH 4.5.

469 **4. Conclusions**

470 This study investigated the interaction of whey protein isolate with the soluble fraction of almond
471 gum at varying biopolymer ratio, pH, and total polymer concentration, which indicated that the
472 interaction was primarily electrostatic. The selected conditions for the formation of the soluble
473 complexes were a total concentration of 0.4 % w/v, a WPI:SFAG ratio of 3:2, and pH 4.5. These
474 negatively charged soluble complexes (-36.5 mV) with average size of around 313 nm were used to
475 fabricate thymol Pickering stabilized emulsions. Cryo-SEM and CLSM revealed that the adsorption of
476 the nanoparticles on the surface of the oil droplets was responsible for the stabilization of the thymol
477 emulsions. Droplet size analyses suggested that the WPI-SFAG complexes were successfully capable

to retard aggregation and/or coalescence of the droplets while native WPI showed severe creaming and coalescence after 40 days of storage. The formulated thymol oil-in-water emulsions have a potential application as an antimicrobial and antioxidant agent in different products.

**Acknowledgements**

Hercules Foundation is acknowledged for its financial support in the acquisition of the Scanning Electron Microscope JEOL JSM-7100F equipped with cryo-transfer system (grant number: AUGE-09-029). We would like to thank Benny Lewille for his kind help in SEM image recording. We also acknowledge the help of Bart Roman and Pieter Zwaenepoel from the SynBioC research group during NMR measurements.

## References


Akhtar, M., & Dickinson, E. (2007). Whey protein–maltodextrin conjugates as emulsifying agents: An alternative to gum arabic. *Food Hydrocolloids, 21*(4), 607-616.

AOAC. (2003). Official methods of analysis of AOAC International. In: [Gaithersburg, Md.] : AOAC International.

Castellani, O., Belhomme, C., David-Briand, E., Guérin-Dubiard, C., & Anton, M. (2006). Oil-in-water emulsion properties and interfacial characteristics of hen egg yolk phosvitin. *Food Hydrocolloids, 20*(1), 35-43.

Cui, S. W. (2005). *Food Carbohydrates: Chemistry, Physical Properties, and Applications*: CRC Press

de Castro, R. D., de Souza, T. M. P. A., Bezerra, L. M. D., Ferreira, G. L. S., de Brito Costa, E. M. M., & Cavalcanti, A. L. (2015). Antifungal activity and mode of action of thymol and its synergism with nystatin against Candida species involved with infections in the oral cavity: an in vitro study. *BMC Complementary and Alternative Medicine, 15*, 417.

de Kruif, C. G., Weinbreck, F., & de Vries, R. (2004). Complex coacervation of proteins and anionic polysaccharides. *Current Opinion in Colloid & Interface Science, 9*(5), 340-349.

Deng, L.-L., Taxipalati, M., Que, F., & Zhang, H. (2016). Physical characterization and antioxidant activity of thymol solubilized Tween 80 micelles. *Nature, 6*, 38160.

Dickinson, E. (1998). Stability and rheological implications of electrostatic milk protein–polysaccharide interactions. *Trends in Food Science & Technology, 9*(10), 347-354.

Dickinson, E. (2005). Protein–Polysaccharide Interactions in Food Colloids. In E. Dickinson & P. Walstra (Eds.), *Food Colloids and Polymers* (pp. 77-93): Woodhead Publishing.

Eghbal, N., & Choudhary, R. (2018). Complex coacervation: Encapsulation and controlled release of active agents in food systems. *LWT, 90*, 254-264.

Ettelaie, R., & Murray, B. S. (2015). Evolution of bubble size distribution in particle stabilised bubble dispersions: Competition between particle adsorption and dissolution kinetics. *Colloids and Surfaces A: Physicochemical and Engineering Aspects, 475*, 27-36.

Ettelaie, R., Zengin, A., & Lishchuk, S. V. (2017). Novel food grade dispersants: Review of recent progress. *Current Opinion in Colloid & Interface Science, 28*, 46-55.

Izumi, K. (1977). Proton NMR Spectra of Peracetylated D-Galactopyranose Derivatives in the Presence of Lanthanide Shift Reagents. *The Journal of Biochemistry, 81*(6), 1605-1611.

Kang, S.-H., Y-S., K., E-K., K., Hwang, J.-W., Jeong, J.-H., Dong, X., Lee, J.-W., Moon, S.-H., Jeon, B.-T., & Park, P.-J. (2016). Anticancer Effect of Thymol on AGS Human Gastric Carcinoma Cells. *Journal of Microbiology and Biotechnology, 26*(1), 28-37.

Karácsonyi, Š., Kováčik, V., Alföldi, J., & Kubačková, M. (1984). Chemical and 13C-n.m.r. studies of an arabinogalactan from Larix sibirica L. *Carbohydrate Research, 134*(2), 265-274.

Li, C., Li, Y., Sun, P., & Yang, C. (2013). Pickering emulsions stabilized by native starch granules. *Colloids and Surfaces A: Physicochemical and Engineering Aspects, 431*, 142-149.

Li, J., Chang, J. W., Saenger, M., & Deering, A. (2017). Thymol nanoemulsions formed via spontaneous emulsification: Physical and antimicrobial properties. *Food Chemistry, 232*, 191-197.

Liolios, C. C., Gortzi, O., Lalas, S., Tsaknis, J., & Chinou, I. (2009). Liposomal incorporation of carvacrol and thymol isolated from the essential oil of Origanum dictamnus L. and in vitro antimicrobial activity. *Food Chemistry, 112*(1), 77-83.

Liu, J., Shim, Y. Y., Wang, Y., & Reaney, M. J. T. (2015). Intermolecular interaction and complex coacervation between bovine serum albumin and gum from whole flaxseed (Linum usitatissimum L.). *Food Hydrocolloids, 49*, 95-103.

Lu, X., Zhang, H., Li, Y., & Huang, Q. (2018). Fabrication of milled cellulose particles-stabilized Pickering emulsions. *Food Hydrocolloids, 77*, 427-435.

Mahfoudhi, N., Chouaibi, M., Donsì, F., Ferrari, G., & Hamdi, S. (2012). Chemical composition and functional properties of gum exudates from the trunk of the almond tree (Prunus dulcis). *Food Science and Technology International, 18*(3), 241-250.

McClements, D. J., & Gumus, C. E. (2016). Natural emulsifiers—Biosurfactants, phospholipids,

biopolymers, and colloidal particles: Molecular and physicochemical basis of functional performance. *Advances in colloid and interface science, 234*, 3-26.
Nosalova, G., Jurecek, L., Chatterjee, U. R., Majee, S. K., Nosal, S., & Ray, B. (2013). Antitussive Activity of the Water-Extracted Carbohydrate Polymer from Terminalia chebula on Citric Acid-Induced Cough. *Evidence-Based Complementary and Alternative Medicine, 2013*, 7.
Pelegrine, D. H. G., & Gasparetto, C. A. (2005). Whey proteins solubility as function of temperature and pH. *LWT - Food Science and Technology, 38*(1), 77-80.
Rezaei, A., Nasirpour, A., & Tavanai, H. (2016). Fractionation and some physicochemical properties of almond gum (Amygdalus communis L.) exudates. *Food Hydrocolloids, 60*, 461-469.
Sedaghat Doost, A., Devlieghere, F., Dirckx, A., & Van der Meeren, P. (2018). Fabrication of Origanum compactum essential oil nanoemulsions stabilized using Quillaja Saponin biosurfactant. *Journal of Food Processing and Preservation, 42*(7), e13668.
Sedaghat Doost, A., Dewettinck, K., Devlieghere, F., & Van der Meeren, P. (2018). Influence of non-ionic emulsifier type on the stability of cinnamaldehyde nanoemulsions: A comparison of polysorbate 80 and hydrophobically modified inulin. *Food Chemistry, 258*, 237-244.
Sedaghat Doost, A., Muhammad, D. R. A., Stevens, C. V., Dewettinck, K., & Van der Meeren, P. (2018). Fabrication and characterization of quercetin loaded almond gum-shellac nanoparticles prepared by antisolvent precipitation. *Food Hydrocolloids, 83*, 190-201.
Sedaghat Doost, A., Sinnaeve, D., De Neve, L., & Van der Meeren, P. (2017). Influence of non-ionic surfactant type on the salt sensitivity of oregano oil-in-water emulsions. *Colloids and Surfaces A: Physicochemical and Engineering Aspects, 525*, 38-48.
Semenova, M. (2017). Protein–polysaccharide associative interactions in the design of tailor-made colloidal particles. *Current Opinion in Colloid & Interface Science, 28*, 15-21.
Setiowati, A. D., Saeedi, S., Wijaya, W., & Van der Meeren, P. (2017). Improved heat stability of whey protein isolate stabilized emulsions via dry heat treatment of WPI and low methoxyl pectin: Effect of pectin concentration, pH, and ionic strength. *Food Hydrocolloids, 63*, 716-726.
Simas-Tosin, F. F., Wagner, R., Santos, E. M. R., Sassaki, G. L., Gorin, P. A. J., & Iacomini, M. (2009). Polysaccharide of nectarine gum exudate: Comparison with that of peach gum. *Carbohydrate Polymers, 76*(3), 485-487.
Su, D., & Zhong, Q. (2016). Formation of thymol nanoemulsions with combinations of casein hydrolysates and sucrose stearate. *Journal of Food Engineering, 179*, 1-10.
Turgeon, S. L., Beaulieu, M., Schmitt, C., & Sanchez, C. (2003). Protein–polysaccharide interactions: phase-ordering kinetics, thermodynamic and structural aspects. *Current Opinion in Colloid & Interface Science, 8*(4), 401-414.
Van der Meeren, P., El-Bakry, M., Neirynck, N., & Noppe, P. (2005). Influence of hydrolysed lecithin addition on protein adsorption and heat stability of a sterilised coffee cream simulant. *International dairy journal, 15*(12), 1235-1243.
Wagoner, T. B., & Foegeding, E. A. (2017). Whey protein–pectin soluble complexes for beverage applications. *Food Hydrocolloids, 63*, 130-138.
Wang, X.-Y., & Heuzey, M.-C. (2016). Pickering emulsion gels based on insoluble chitosan/gelatin electrostatic complexes. *RSC Advances, 6*(92), 89776-89784.
Wei, Z., Zhu, P., & Huang, Q. (2018). Investigation of ovotransferrin conformation and its complexation with sugar beet pectin. *Food Hydrocolloids*.
Wijaya, W., Van der Meeren, P., Wijaya, C. H., & Patel, A. R. (2017). High internal phase emulsions stabilized solely by whey protein isolate-low methoxyl pectin complexes: effect of pH and polymer concentration. *Food & Function, 8*(2), 584-594.
Willför, S., Sjöholm, R., Laine, C., & Holmbom, B. (2002). Structural features of water-soluble arabinogalactans from Norway spruce and Scots pine heartwood. *Wood Science and Technology, 36*(2), 101-110.
Wu, J., Shi, M., Li, W., Zhao, L., Wang, Z., Yan, X., Norde, W., & Li, Y. (2015). Pickering emulsions stabilized by whey protein nanoparticles prepared by thermal cross-linking. *Colloids and*

*Surfaces B: Biointerfaces, 127*, 96-104.
Xiao, J., Li, Y., & Huang, Q. (2016). Recent advances on food-grade particles stabilized Pickering emulsions: Fabrication, characterization and research trends. *Trends in Food Science & Technology, 55*, 48-60.
Yanishlieva, N. V., Marinova, E. M., Gordon, M. H., & Raneva, V. G. (1999). Antioxidant activity and mechanism of action of thymol and carvacrol in two lipid systems. *Food Chemistry, 64*(1), 59-66.
Ye, A. (2008). Complexation between milk proteins and polysaccharides via electrostatic interaction: principles and applications – a review. *International Journal of Food Science & Technology, 43*(3), 406-415.

a)

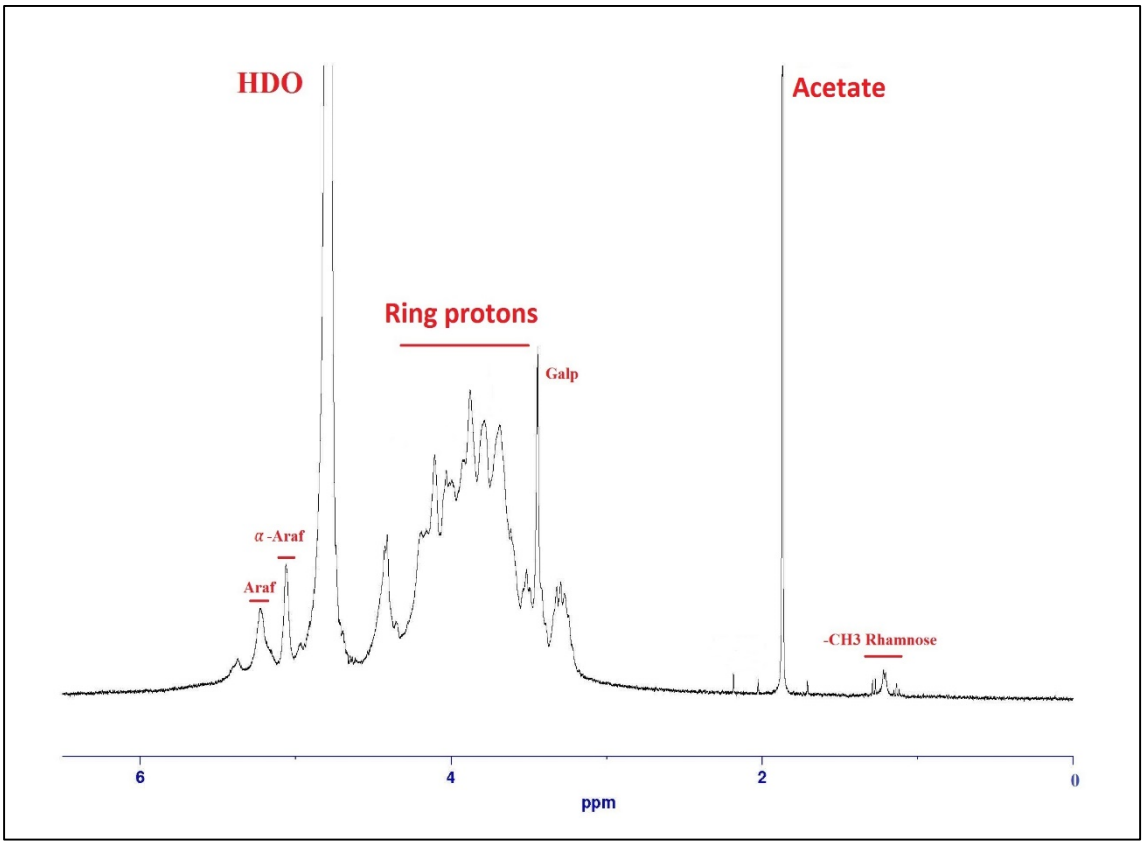


b)

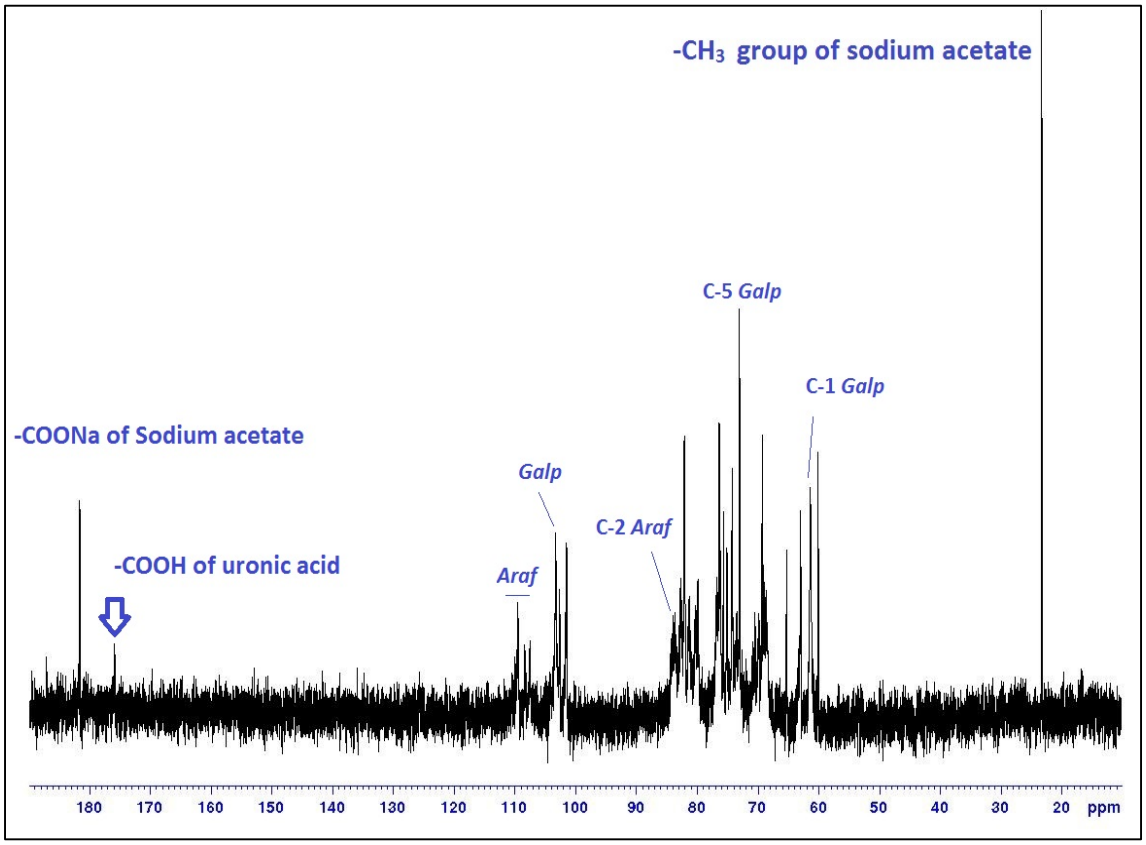


*Figure 1. 1-D $^{1}$H- (a) and $^{13}$C-NMR (b) spectra of the water soluble fraction of almond gum containing sodium acetate as an internal standard recorded at 30°C.*

a)

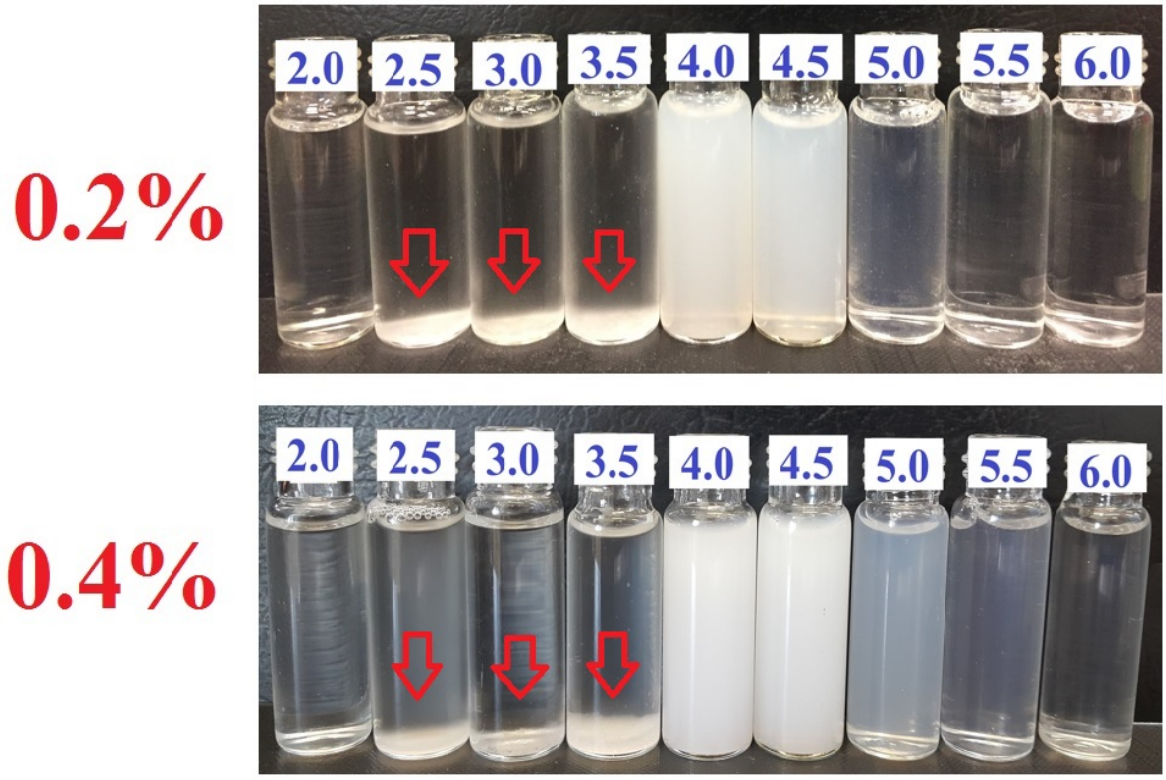


b)

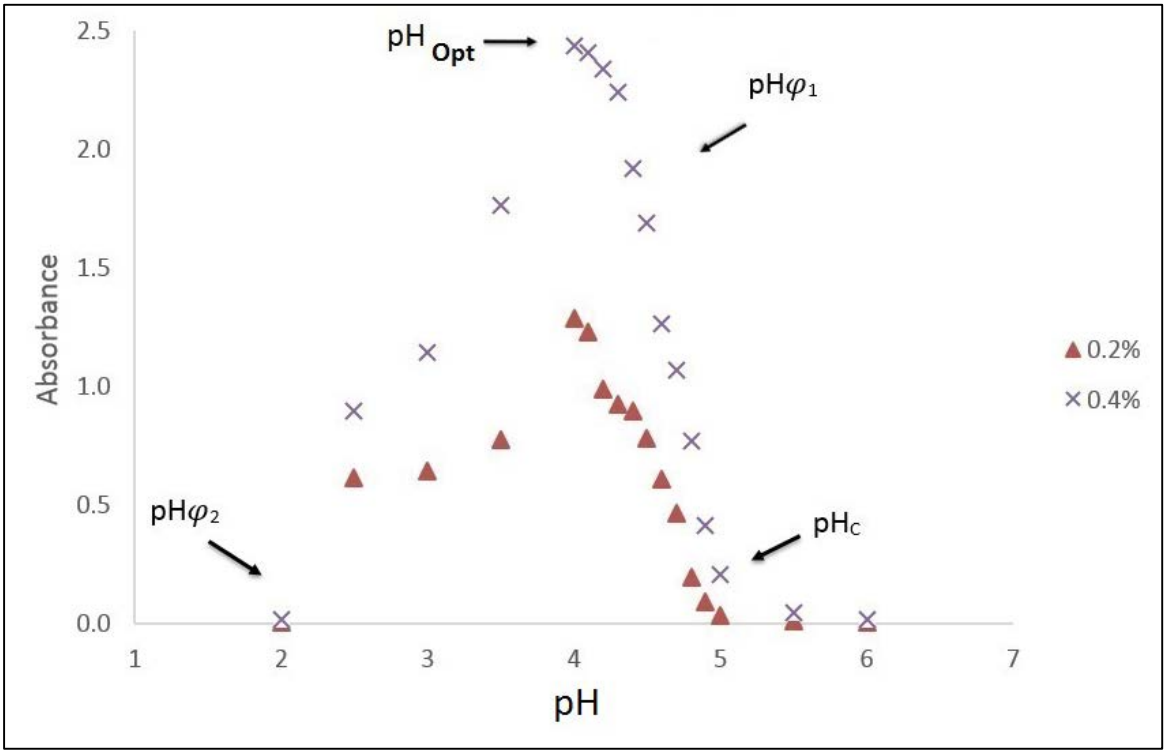


*Figure 2. Optical appearance (a) and optical density (600nm) (b) of whey protein isolate-soluble fraction of almond gum complexes (3:2) at two different total biopolymer concentrations (0.2 and 0.4%w/v) as a function of pH.*

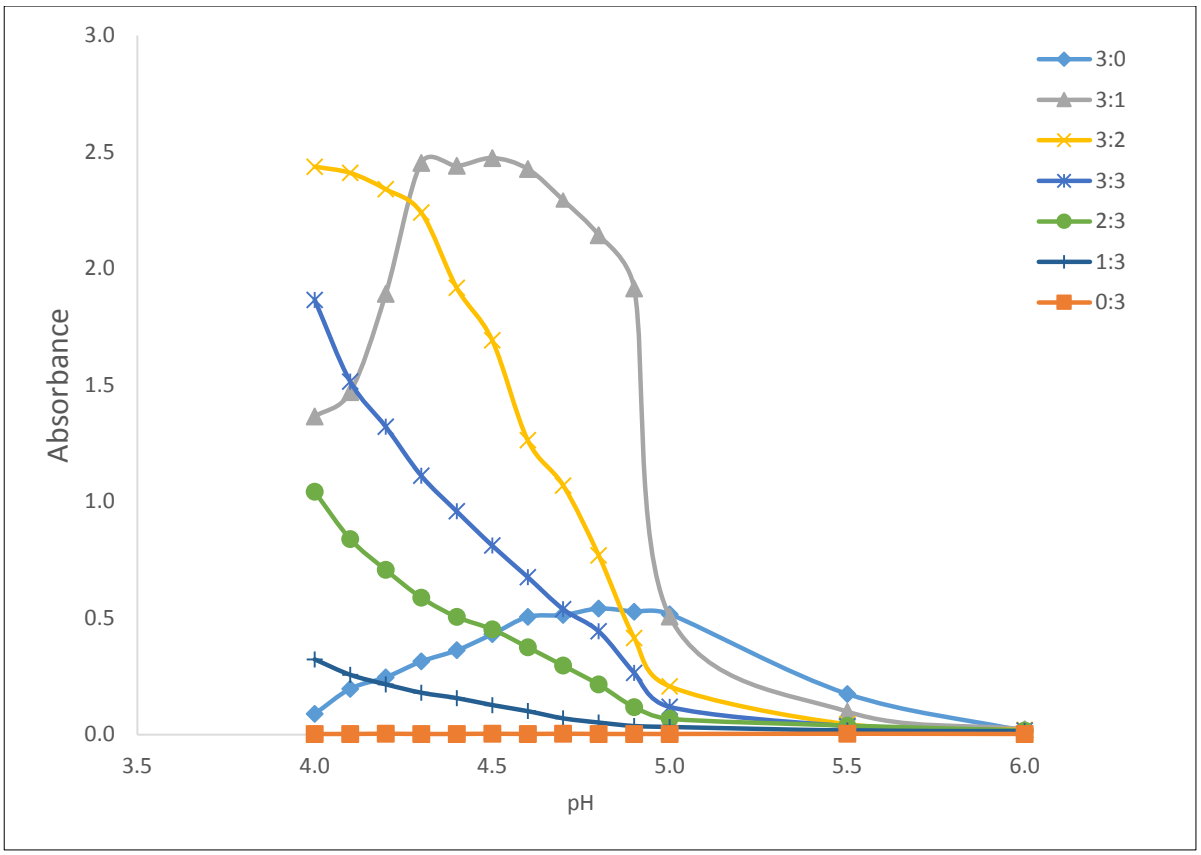


*Figure 3. Influence of whey protein isolate and soluble fraction of almond gum ratio at constant total concentration (0.4%w/v) on the optical density (600nm) of the formed complexes at variable pH conditions (4-6).*

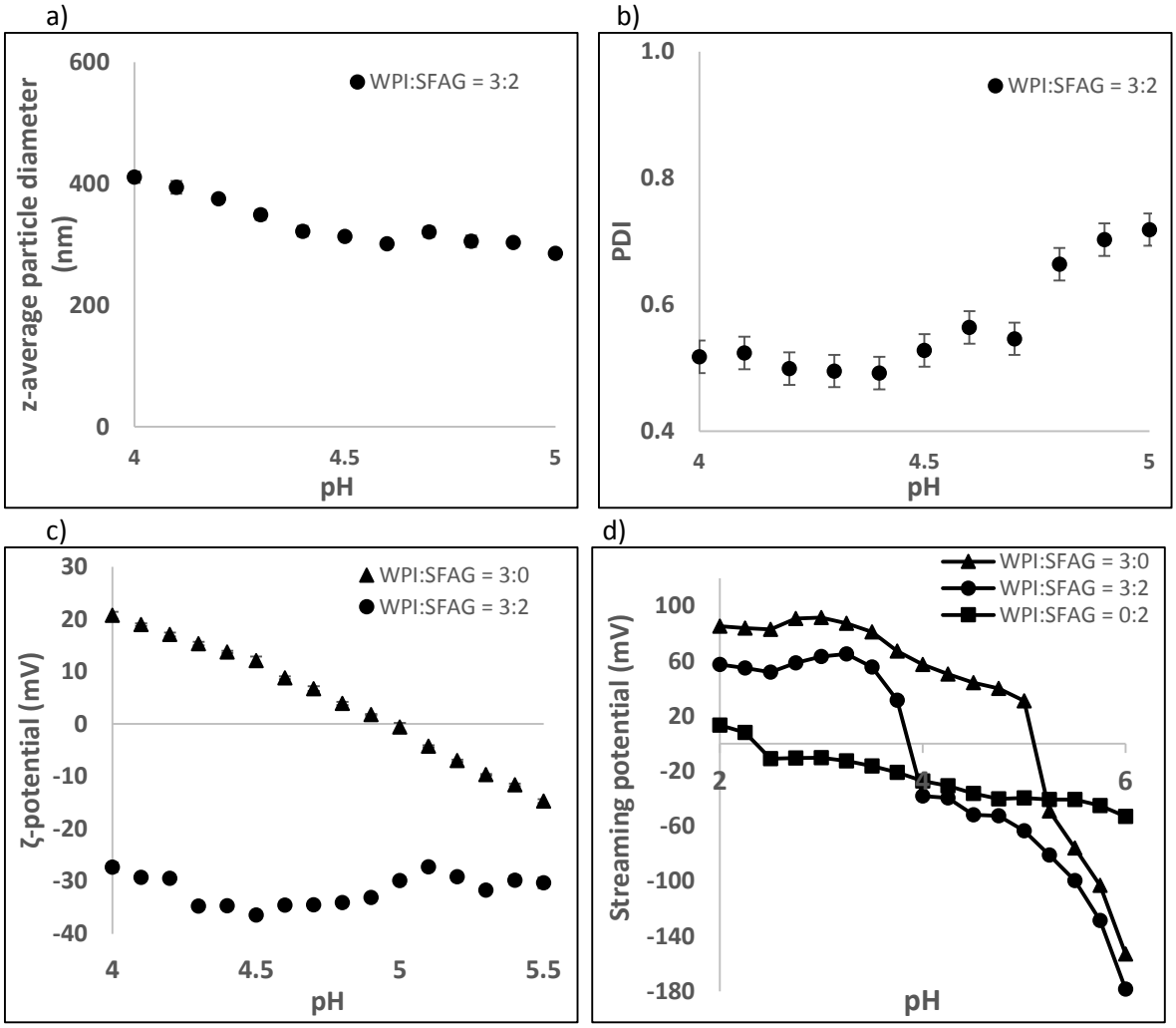


*Figure 4. Evolution of particle size (a), polydispersity index (PDI) (b), zeta-potential (c), and streaming potential (d) of whey protein isolate (WPI) – soluble fraction of almond gum (SFAG) complexes (ratio = 3:2, TC = 0.4%w/v) as a function of pH; for comparison, native WPI (c and d) and SFAG (d) were included.*

**a)**

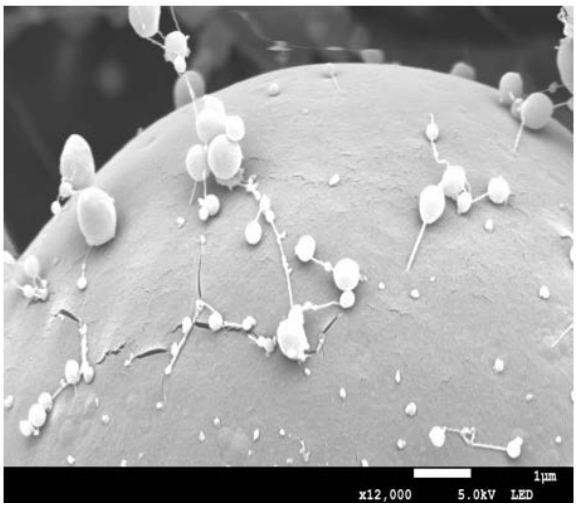


**b)** **c)**

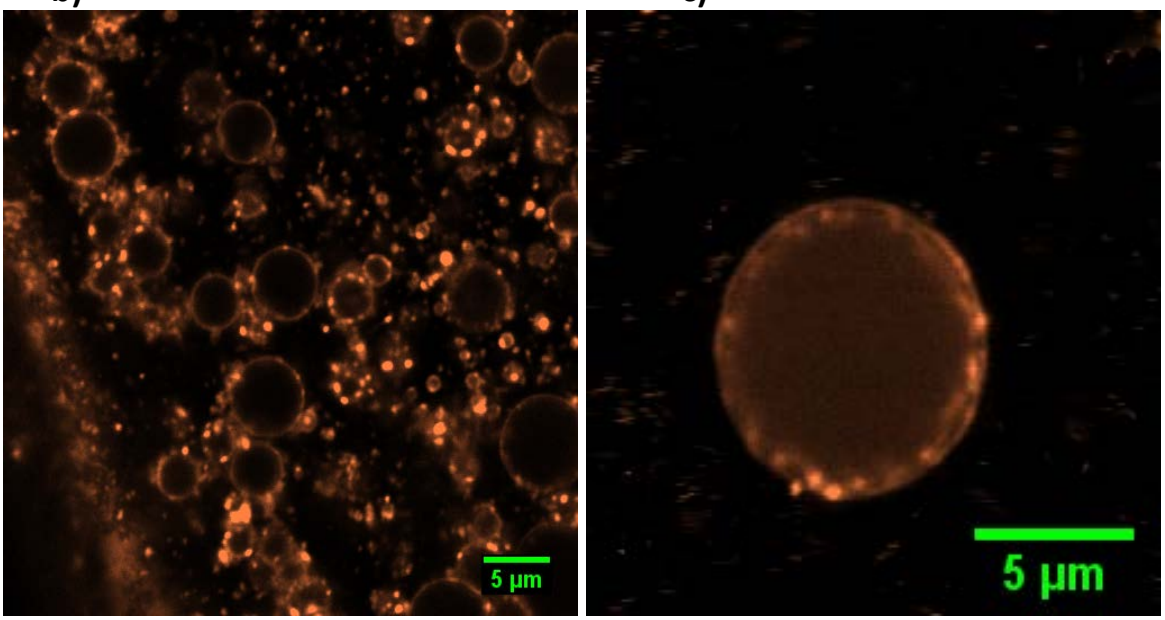


*Figure 5. Cryo-SEM photograph (a) and CLSM in Rhodamine B detection mode of undiluted (b) and diluted (c) of 4% thymol emulsions stabilized by whey protein isolate-soluble fraction of almond gum particles (ratio = 3:2, TC = 0.4%w/v) prepared at 10mM sodium acetate buffer (pH 4.5) (the pictures were taken at day 0).*

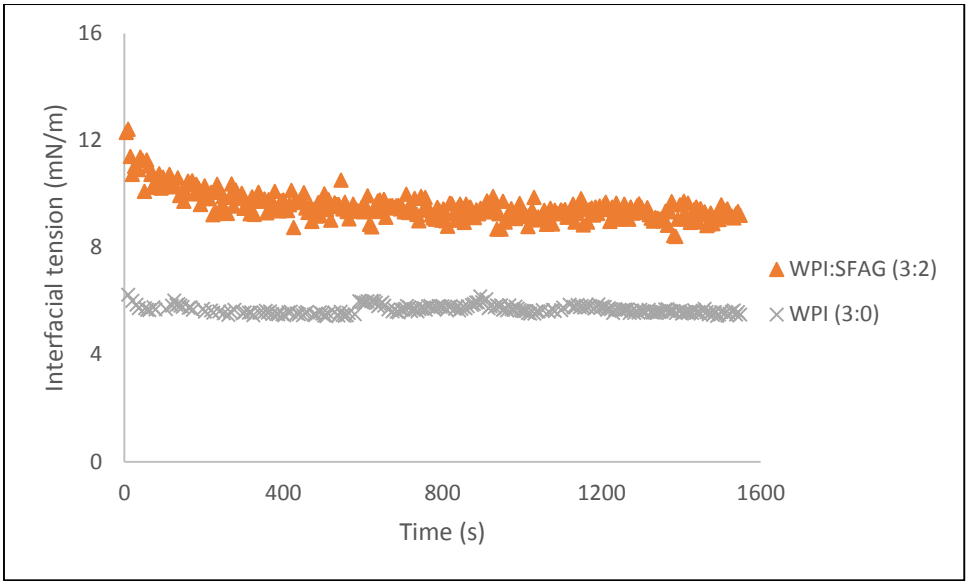


*Figure 6. Interfacial tension variation between an aqueous phase containing either native whey protein isolate (WPI) or WPI-soluble fraction of almond gum (SFAG) particles (TC = 0.4%w/v) and thymol mixed with tricaprilyn oil (4:1) at 25°C.*

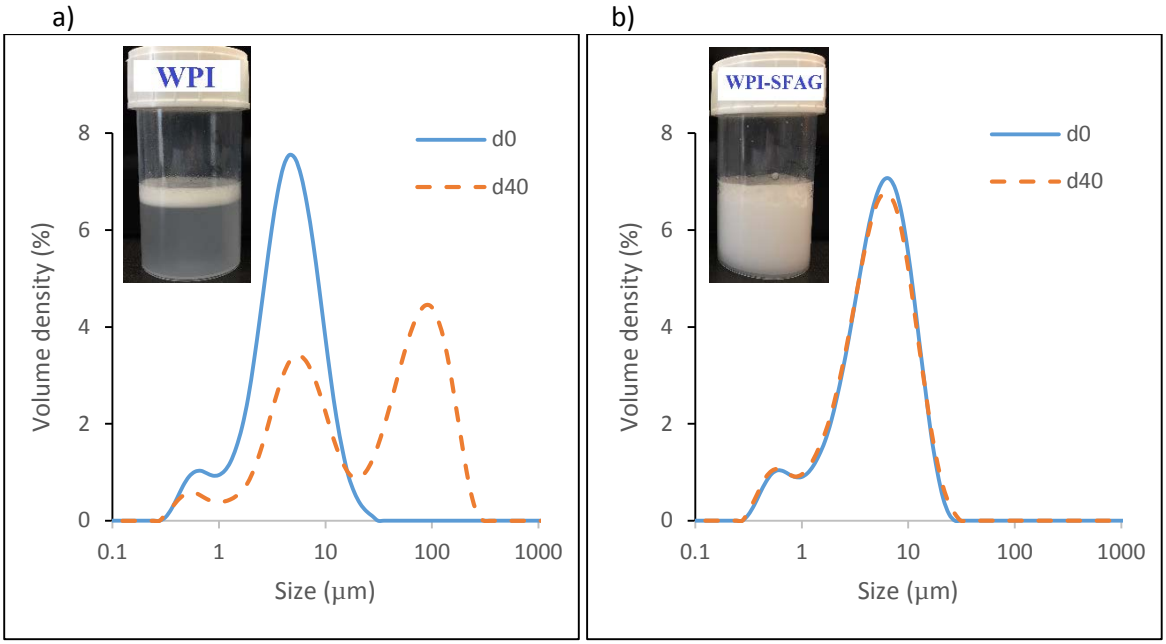


*Figure 7. Volume-weighted droplet size distribution of thymol emulsions stabilized using either native whey protein isolate (WPI) (a) or WPI- soluble fraction of almond gum (SFAG) complexes (b) at a ratio of 3:2 (total concentration = 0.4%w/v) after 0 and 40 days of storage at 4°C.*